Ice volume and basal topography estimation using geostatistical methods and GPR measurements: Application on the Tsanfleuron and Scex Rouge glacier, Swiss Alps

Alexis Neven[1,*], Valentin Dall'Alba[1,*], Przemysław Juda[1], Julien Straubhaar[1], and Philippe Renard[1,2]

[1]Centre of Hydrogeology and Geothermics, University of Neuchâtel, Switzerland
[2]Department of Geosciences, University of Oslo, Oslo, Norway
[*]These authors contributed equally to this work.

Correspondence: Alexis Neven (alexis.neven@unine.ch)

Abstract. Ground Penetrating Radar (GPR) is nowadays widely used for determining glacier thickness. However, this method provides thickness data only along the acquisition lines and therefore interpolation has to be made between them. Depending on the interpolation strategy, calculated ice volumes can differ and can lack an accurate error estimation. Furthermore, glacial basal topography is often characterized by complex geomorphological features, which can be hard to reproduce using classical interpolation methods, especially when the conditioning data are sparse or when the morphological features are too complex. This study investigates the applicability of multiple-point statistics (MPS) simulations to interpolate glacier bedrock topography using GPR measurements. In 2018, a dense GPR data set was acquired on the Tsanfleuron Glacier (Switzerland). The results obtained with the direct sampling MPS method are compared against those obtained with kriging and sequential Gaussian simulations (SGS) on both a synthetic data set – with known reference volume and bedrock topography – and the real data underlying the Tsanfleuron glacier. Using the MPS modelled bedrock, the ice volume for the Scex Rouge and Tsanfleuron Glacier is estimated to be 113.9 ± 1.6 Miom^3. The direct sampling approach, unlike the SGS and the kriging, allowed not only an accurate volume estimation but also the generation of a set of realistic bedrock simulations. The complex karstic geomorphological features are reproduced, and can be used to significantly improve for example the precision of under-glacial flow estimation.

1 Introduction

It is widely accepted that global climatic changes are impacting future precipitation rates and temperatures. In Switzerland, these changes will inevitably induce new stresses on alpine environments and on glacier mass balance. In this context, the monitoring of glacier thickness and volume is crucial, in order to predict the rate of their melting and the possible consequences on both water resources, sediment production, and slope stabilization.

The Cryosphere
Discussions

Ice volume estimation relies on two components : (1) the surface topography of the glacier and (2) the underlying bedrock topography. The first one is easily measurable using either LIDAR (e.g. Haugerud et al., 2003), satellite measures (e.g. Berthier et al., 2014) or uncrewed aerial vehicle (e.g. Chudley et al., 2019). However, the variations in basal topography are difficult to measure, due to the impossibility of reaching it easily with direct measurements. Ground Penetrating Radar (GPR) is nowadays

25 widely used for determining the thickness of the ice mass (Flowers and Clarke, 1999; Plewes and Hubbard, 2001; Bohleber et al., 2017). The equipment has the advantage of being light and easy to use in a glacial environment. However, this method only provides thickness data along the acquisition lines and therefore interpolation methods are needed to estimate the basal topography. Depending of the interpolation methods, the basal topography can change significantly and can lead to a wide range of calculated ice volumes. Moreover, some of the methods generally used can lack to provide an accurate error esti-

30 mation. Furthermore, if we are interested in the basal topography to simulate subglacial flow, for example, the choice of the method becomes critical since the flow process is highly non-linear and is strongly linked to the morphology of the subglacial topography.

One classical interpolation strategy used for basal estimation is the ordinary kriging method (e.g. Vanlooy et al., 2014). This method provides fast and reliable interpolation of the data and returns the best linear unbiased estimator. The kriging estimation

35 produces by construction a smooth interpolation and does not represent the possible detailed morphology of the bedrock when it is not constrained by sufficient data. Furthermore, even if kriging allows estimation of the local uncertainty on the elevation of the bedrock, it cannot be used to estimate the uncertainty of the global volume of ice (see e.g. Chiles and Delfiner, 2012, p. 478). Stochastic simulations using Gaussian processes have the opposite aim to represent the variability and spatial statistics of the basal morphology (Goff et al., 2014), which are important because they affect the topographic resistance to glacier flow.

40 Furthermore, the simulations can be used for uncertainty estimations. A downside of these two methods is that they are based on two points spatial statistics (covariance or variogram models) and use a multi-Gaussian assumption, implying that they cannot succeeded to simulate complex spatial patterns when the data are not sufficiently dense.

Other empirical methods using volume-area (V-A) relations are also used to calculate ice volume. These methods includes slope-dependent volume estimation, ice thickness distribution (e.g. Frey et al., 2014) or surface velocity estimation (e.g. Gan-

45 tayat et al., 2014). V-A estimation methods are based on the observation that larger glaciers tend to be thicker than smaller ones. These methods are easy and fast to apply. However, they generally lack spatial uncertainty analysis and can be very sensitive to their parametrization processes. Their applications result in a single ice volume estimation, which does not allow to capture the uncertainty of the model. Finally, they only produce an estimation of the thickness of the glacier and cannot help to predict underground topography.

50 In the last decades, new geostatistical methods have arisen with the aim to improve the realism of the simulation using another form of information that the one expressed by two points statistics and variogram interpretation. Multiple-point statistics (MPS) simulation algorithms use a training image (TI) to infer the spatial statistics of the model and generate random fields reproducing these spatial statistics. The TI represents a conceptual knowledge of the variable that is aimed to be simulated, it can be created by experts or can be extracted from analog data sets. Unlike other geostatistical approaches, MPS does not

55 require to define an analytical two-point statistics model to represent the spatial variability but instead infers it in an implicit way
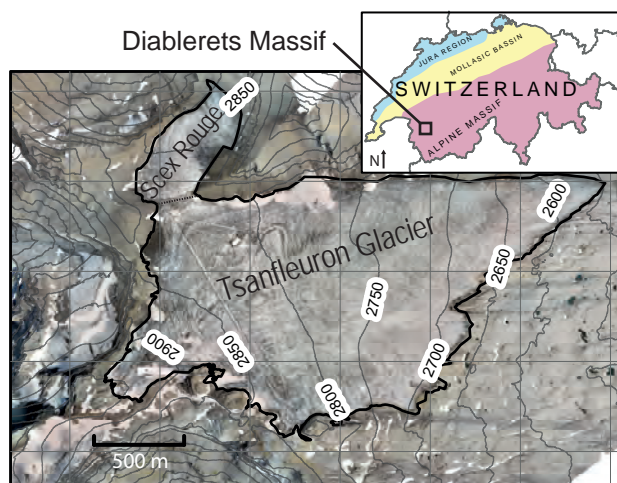
Figure 1. Aerial image and Digital Elevation Model captured from Drone images of the Glacier of Tsanfleuron, Switzerland.

from the TI provided by the user (Journel and Zhang, 2006). MPS simulations benefit from this additional knowledge and can also be constrained by the acquired data (the conditioning data). These methods allow to create more realistic spatial patterns than classical two-points geostatistical methods and can be used to represent the uncertainty by simulating a set of realizations. Some examples of application can be found in Oriani et al. (2014); de Carvalho et al. (2016); Dall'Alba et al. (2020). In recent

60 studies, MPS has successfully been applied to estimate under-glacial topography from synthetic data (MacKie and Schroeder, 2020) and to evaluate the probability of under-glacial lakes (MacKie et al., 2020).

The aims of this paper are both methodological and applied. Regarding the methodological aspect, this work aims to demonstrate the use of the MPS method to combine information provided by GPR data points and Digital Elevation Model (DEM) to simulate a realistic glacial basal topography. The benefits of using a MPS approach are highlighted by comparing its results

65 with those obtained with more classical geostatistical methods. Using synthetic test cases, the different methods are compared by calculating for each one an ice-volume and a roughness estimation, which are then compared against the true synthetic values. A set of scores are computed to compare the methods. Through this comparison process different parameter sets are also tested for each methods. This methodological aspect helps to select the most suitable parameter sets and also illustrate on a case where the reference is known the advantages of the multiple-point simulation approach for estimating glacier volume and its

70 associated basal's geomorphology. On the applied side, the objectives are to present new field data and new estimations of the volume of the Tsanfleuron glacier, roughly 10 years after the last detailed published estimation (Gremaud and Goldscheider, 2010).

The Tsanfleuron glacier and the Scex Rouge glacier (Fig. 1) are both located in the Diablerets Massif (Schoeneich and Reynard, 2021) in Switzerland. They are connected to each other at the Tsanfleuron pass, but lies on two different faces : the

75 main slope of the Scex Rouge glacier is toward the north north-east, while the Tsanfleuron slope is toward the east. Tsanfleuron volume was estimated to be $100\,\mathrm{mio\,m}^3$ of ice in 2009 using radio-magneto-telluric data and kriging of the ice thickness, with

3

The Cryosphere

Discussions

Open Access

EGU

an uncertainty of ±10% and a maximum measured depth of 138 m (Gremaud and Goldscheider, 2010). According to their measurements, the glacier is currently losing about 1.5 m of thickness per year. A more recent publication, applied on all Swiss glaciers, proposed a volume for Tsanfleuron and Scex Rouge of respectively 200.02 and 8.12 $\mathrm{mio\,m^3}$ in 2016 (Grab et al.,

80   2021). However, the uncertainty on the GPR picking used in the particular case of Tsanfleuron is important, especially with thicknesses bigger than 60 m according to a personal communication with one of the author. Both glaciers lie on carbonate formations that are heavily karstified. The glacier is one of the main feeders of the underlying karstic system. Tracers tests showed that this network is a significant source of drinking water supply for the community of Conthey (Gremaud, 2008). Obtaining a better model of the basal topography is therefore a step toward improving the understanding of the remaining ice

85   volume, the glacial retreat behavior, and its impact on the regional groundwater system.

The core MPS technique used in this study is the direct sampling algorithm (Mariethoz et al., 2010) implemented in the DeeSse code (Straubhaar, 2019). This implementation includes several improvements as compared to the original algorithm, in particular DeeSse can account for multi-resolution structures in the data set (Straubhaar et al., 2020) and inequality data (Straubhaar and Renard, 2021).

90   In this paper, the exposed basal surface of the melted glacier zones is employed as a training image for the simulation of the covered glacier basal topography. The justification for this modeling decision is that the lithology and general topographical slope below the glacier and in the exposed area are similar, and therefor the geomorphological features should also be similar. This idea is validated by the analysis of the area where the glacier retreated in the last dozen years, which exposed geomorphological structures similar to the older part. The GPR inferred depths are then used as conditioning points as well as the

95   topographical data around the glacier.

Since the exact topography below the glacier is unknown, to analyze and benchmark the performances of different interpolation methods, a numerical experiments must be designed in which references can be compared to the simulation outputs. For that purpose, the exposed part of the bedrock is also used (besides being used as TI) to compare the performances of the MPS, kriging, and sequential Gaussian simulation (SGS) approaches. 20 zones are extracted from the exposed DEM and sampled

100   to create fake GPR data sets. Using only the sampled data set, the topography in the test zones are interpolated using MPS, SGS, and kriging and compared to the reference topography. The absolute volume is also analysed. In addition, since some parameters must be defined for all the geostatistical methods, different parameters sets are tested for each method through this experiment. Finally, different scores are used to compare the methods. This numerical experiment helps to understand and visualize the impact of each method on the simulated bedrock shape and volume estimation distribution.

105   Lastly, the Tsanfleuron and Scex Rouge bedrock topography is interpolated using the previously tested methods and parameters sets. A brief overview of the glacier volume distributions and their evolution through past time is finally carried out using the calculated bedrock surfaces and different DEM.

2 Methods

2.1 GPR and DEM acquisition

110   In summer 2018, a dense GPR acquisition on the Tsanfleuron glacier was performed (Fig. 2) using a single Radarteam Cobra GPR antenna of 80 Mhz centre-frequency, mounted on a backpack with a RTK differential GPS. Total listening time was set to 1600 ns with a sample rate of 320 MHz. The GPR data were processed using a standard workflow. A time-zeroing was performed, setting the origin of the time vector when the first arrival is recorded. Our system being a single antenna system, this time corresponds in fact to the recording of the pulse itself. We then apply a time dependant gain, being the time vector

115   risen to a power 1.2. A de-wow filter was also added, using the residual median filter method described in Gerlitz et al. (1993). We then removed the mean trace to avoid displaying the pulse and the airwave present in all the traces. Finally, a 120 MHz low pass filter was applied to remove the signals outside of the GPR band. The data were binned in a 2 m grid. The time to depth conversion was done using a uniform wave propagation speed of 0.168 m/ns (Eisen et al., 2002; Moorman and Michel, 2000). The basal reflector identification and the picking was then performed multiple times, with a random display of the

120   lines, by four different operators. The random selection of the line was done in order to avoid bias and over interpretation of the GPR data reflections. The processing was identical for all operators, however they had the possibility to adapt the display (colormap and percentile clipping). All of the picked points which showed differences of more than 5 meters between the different operators were considered as unsure and therefore rejected. This resulted in a good basal depth estimation in 87 % of the lines. As expected, the deepest zones (more than 70 - 80 m) are the most difficult to identify precisely, with a smaller noise

125   to signal ratio. A exemple line is display on Fig.2. The data were then converted to a point set, representing the position of the measurement and the altitude of the basal reflector, to be used with the MPS algorithm.

In addition, during the summer in 2019 several UAV flights were realized above the Tsanfleuron glacier. We conducted 5 flights with a Sense Fly EBEE UAV equipped with a 20-megapixel RGB camera. The objective was to have a resolution of at least 10 cm/pixel everywhere on the glacier, and an overlap of 60 % between the images. The resulting flight altitude was

130   between 300 m to 600 m above ground. A DEM and an orthomosaic (Fig. 1) were generated using a stereoscopic method, and the whole domain was geolocated using Ground Control Points. The image processing was done using the Pix4D software.

2.2 Multiple-Point Simulation

The MPS algorithm used in this paper is *DeeSse* (Straubhaar, 2019). It is based on the direct sampling technique that is described in detail in Mariethoz et al. (2010). The principle of the method is that a conditional simulation is generated by

135   sampling patterns from a training data set. The simulation is sequential, a random path is used to define in which order the cells of the grid have to be simulated. For each cell, the pattern constituted by the already simulated or conditioning data surrounding the current cell is retrieved. The algorithm then searches in the training data and in a random manner some patterns that are similar to the conditioning pattern. When a similar pattern is found the value at the central location of the pattern is copied from the training data to the simulation grid. This technique allows to co-simulate jointly several variables. The code proposes

140   a set of options such as the relative distance search (Mariethoz et al., 2010) allowing to account for non stationarity of the mean
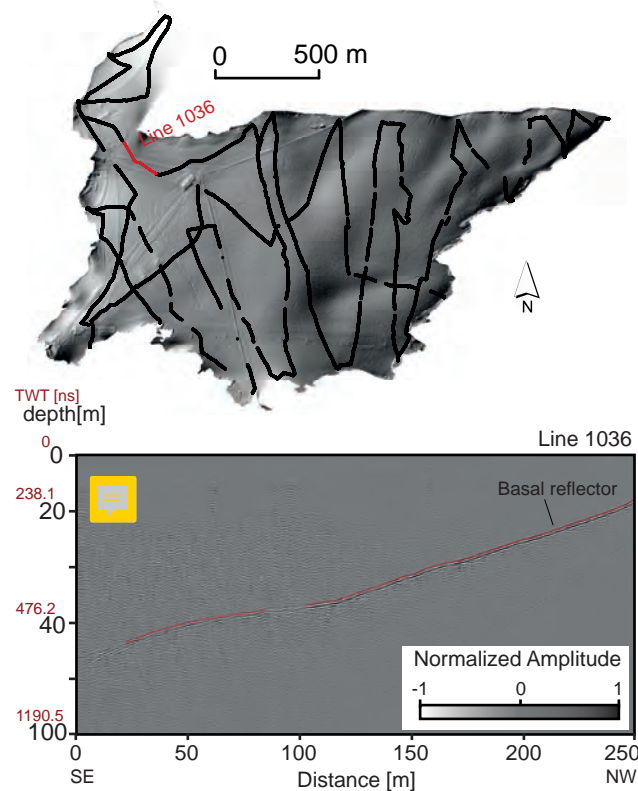
Figure 2. Acquisition lines from August 2018. The cumulative length is about 18km. Hill shade from the DEM derived from Drone images. The straight lines visible on the hill shade are ski lifts and transit tracks for snow groomers. A GPR line is displayed, with the basal reflector outlined.

values in the simulation grid. Furthermore, the *DeeSse* code includes several improvements as compared to the original method such as the use of Gaussian pyramids to account for multiscale patterns (Straubhaar et al., 2020).

The three main parameters of the method are the maximum number of neighbors (n), the distance threshold (t) and the scan fraction (f). n controls how many nodes are used for the pattern comparison between the TI and the simulation grid. t sets
145   the maximum acceptable dissimilarity when comparing a pattern in the simulation grid and in the TI. Finally, f controls the maximal fraction of the TI that can be scanned when searching for a pattern. The optimal values of these parameters depend on the complexity of the pattern that are displayed in the training data set and on the acceptable computing time to obtain a set of simulations. Some recommendations on how to select those parameters are presented in Meerschman et al. (2013).

In the case of the Tsanfleuron glacier, the acquired DEM of the exposed bedrock is used as TI. The hard data are the GPR
150   lines and the altitude of the bedrock (from the DEM) surrounding the glacier. To obtain the best parameters for this data set, a series of experiments with different parameter sets was conducted. The methodology to conduct these tests is described in detail in section 2.4.

For all the simulations, the multiscale mode using Gaussian pyramids and relative distance options are activated to get the best reproduction of the patterns. Furthermore, a secondary variable is used during the MPS simulations. The first feature

155 improves the simulation of patterns at different scales and produces more consistent simulation outputs (Straubhaar et al., 2020). The second feature is a way to deal with non-stationary data sets. Indeed, we are interested here in relative changes of the topography along the altitude. Two patterns that show the same relative changes even at different absolute altitudes should be considered similar. Finally, the computed topography gradient is added as a secondary variable in the TI. This variable is not defined in the hard data set, but it is simulated and it improves the quality of the simulation. These options are fixed for all

160 the synthetic parameters test sets.

2.3 Kriging and SGS

Kriging and sequential Gaussian simulations (SGS) are standard geostatistical techniques that are well described in many textbooks (e.g. Chiles and Delfiner, 2012). Therefore we will not describe here the underlying theory of these methods but rather focus on the specific aspects of their application in our case.

165 At the scale of the study site, the exposed bedrock topography presents a general slope toward the east and is therefore non-stationary. To account for this general slope, we decided to remove first the trend present in the DEM and in the hard (GPR) data before conducting the variogram analysis. To do so, a polynomial surface is fitted and removed from the data. By removing the polynomial surface from the data, only the deviation from this surface, which corresponds to the deviation from the general slope of the glacier, is simulated. At the end of the process, the trend is then added to the interpolated values

170 to obtain the final basal topography. It is important to note that since the Scex Rouge and the Tsanfleuron glaciers have two different orientations, two different trends were interpolated: one was used for the Tsanfleuron glacier and the other one for the Scex rouge glacier. The transition being set at the Tsanfleuron pass. The polynomial interpolated trends being in the form of :

$$f(x,y) = a + bx + cy + dx^2 + exy + fy^2 \tag{1}$$

$$= 0 - 0.281x - 0.143y - 6.09 * 10^{-6}x^2 + 7.98 * 10^{-5}xy - 1.28 * 10^{-5}y^2 \ (Tsanfleuron) \tag{2}$$

175 $$= 0 + 1.78x - 3.37y + 4.63 * 10^{-3}x^2 - 3.26 * 10^{-3}xy + 1.505 * 10^{-3}y^2 \ (ScexRouge) \tag{3}$$

with a, b, c, d, e, f being the coefficient and x and y the coordinate in the plane. The variogram model used for the SGS and kriging approaches is shown in Fig. 3. The data set used for calculating the experimental variogram is shown in Fig. 3a on a map view. It is composed of 7'500 points, 2'500 coming from the acquired GPR data and the other 5'000 points randomly sampled from the TI. This data set presents a distribution centered around -4.08 m with a standard deviation value of 21.2

180 m (Fig. 3b) that is close to Gaussian. We therefore did not apply any variable transform to ensure Gaussianity. The variogram map (Fig. 3c) does not show a strong and significant anisotropy. Therefore, an omni-directional variogram model is selected and adjusted to the experimental variogram data. The model is composed of two components: a spherical structure with a sill value of 344 m^2, a range value of 862 m, and a second exponential structure defined by a sill value of 134 m^2 and a range value of 396 m (Fig. 3d). The sequential Gaussian simulations and kriging are performed using the Ar2gems software.
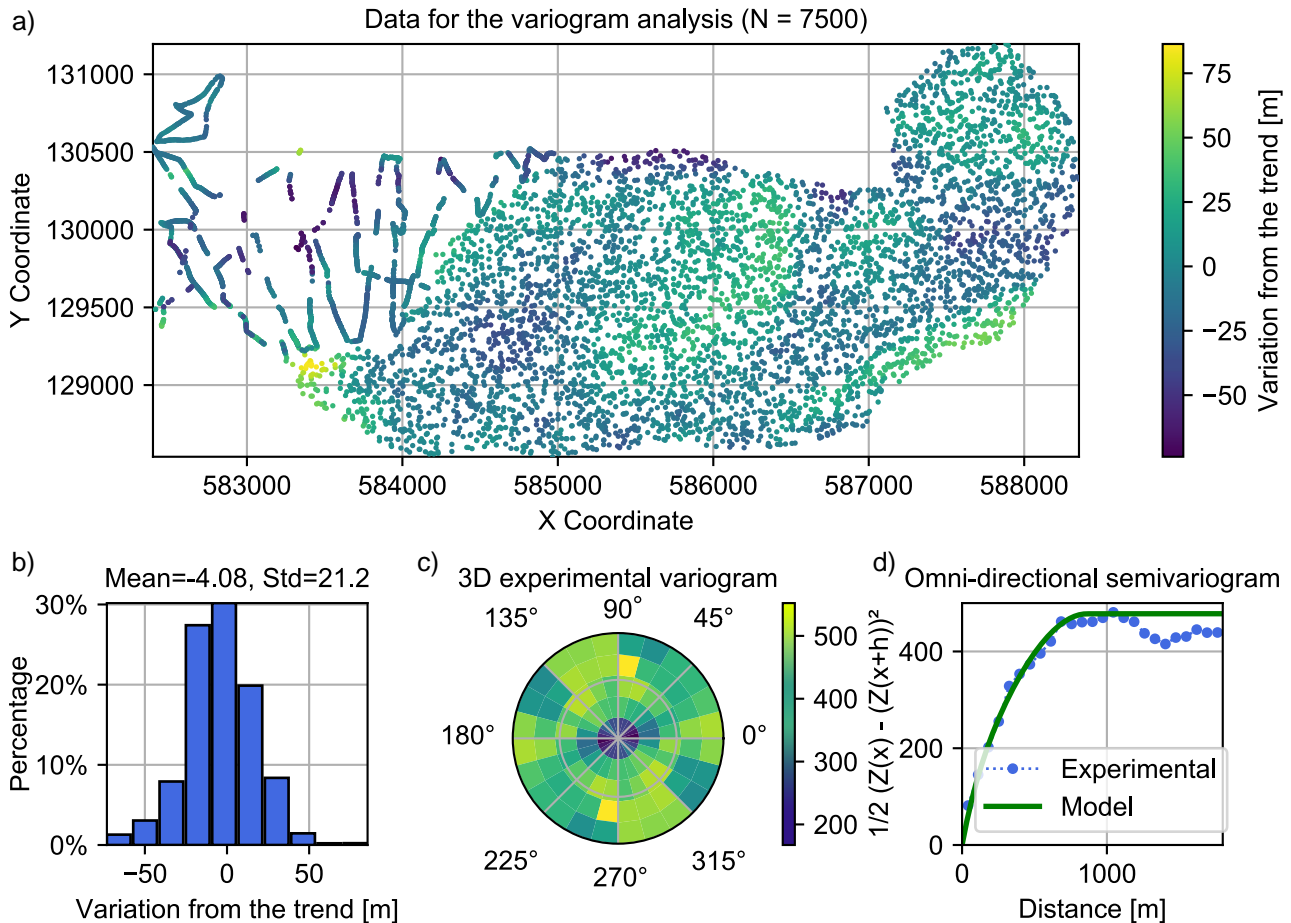
Figure 3. Variogram analysis. a) the data set is composed of 7'500 points and is assumed representative of the spatial variability of the basal topography. b) the data set has an approximate Gaussian distribution centered around −4.08 m, no transformation is applied to it. From the 2D experimental variogram map (c) a 2D omni-directional isotropic model is adjusted against the experimental one (d).

2.4 Systematic comparison of the methods

In order to benchmark the different geostatistical algorithms and parameter sets, a systematic testing approach is applied (Fig. 4). First, the available DEM (the exposed part of the bedrock) is sampled to create 20 synthetic test cases. These are 800×800 m^2 wide zones that are randomly selected in the DEM (Fig. 4). Once the zones are selected, two synthetic GPR acquisition lines are randomly extracted from the topography of each zone. The bed elevation is sampled along the line with a noise and used as conditioning data. The rest of the data is removed. The three interpolation methods are then tested to infer the basal topography. For each zone and for each parameter set: 40 MPS simulations, 40 SGS simulations and one ordinary kriging estimate are performed.
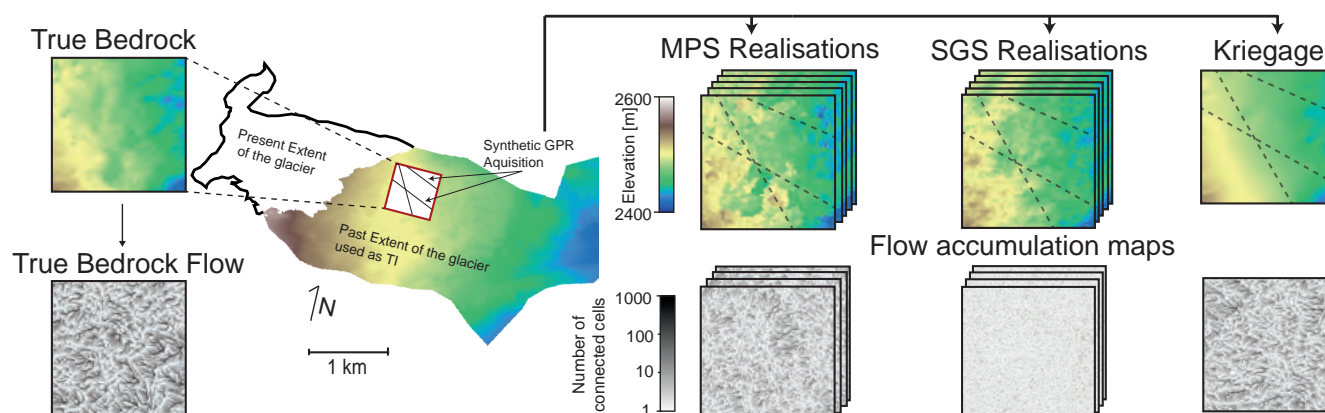
Figure 4. The approach used for the systematic tests. Test zones are extracted from the exposed glacier bedrock. GPR lines are also extracted from these zones and used to constrain the geostatistical simulations. It is then possible to compare the different sets with the actual topography. Flow accumulations maps are calculated from the simulated topography and from the reference extracted DEM for comparison.

Table 1. Parameters sets used for the synthetic tests

Set N°	0	1	2	3	4
n	48	48	48	24	24
t	0.01	0.1	0.05	0.01	0.1

Set N°	5	6	7	8
n	24	12	12	12
t	0.05	0.01	0.1	0.05

For the MPS approach, 9 sets of parameters are considered. They are given in Table 1. The two parameters being tuned are the number of neighbors n, and the distance threshold t. The scan fraction is kept low $f = 0.0005$ because of the size of the training image. Note that if the distance did not reach the threshold during the scan, the best candidate is chosen and the cell is flagged. At the end of the simulation, all the flagged points are re-simulated once.

SGS and ordinary kriging are applied using the same variogram model presented in section 2.3. The simulations and the kriging estimate are conditioned using the synthetic GPR lines. Two SGS sets are generated: the set SGS 1 uses 24 neighbors while the the set SGS 2, uses 40 neighbors. The kriging estimation is realized using 24 neighbors.

Once the simulations are performed, quality indicators are computed from the predicted and actual topography.

The Cryosphere

Discussions

Open Access

2.5 Quality Indicators

The geostatistical methods that are used to interpolate the basal surface can be used to predict accurately certain derived quantities but not some other quantities. To illustrate this idea, quality indicators are defined related to the estimation of the overall ice volume, the estimation of the topography itself, and the estimation of flow accumulation.

205   Another important aspect is that we do not only want to evaluate if the forecasts are close to the reference in average, but we want also to evaluate the quality of the predicted uncertainty ranges. This is why we consider not only the absolute bias but also the continuous ranked probability score (CRPS) (Gneiting et al., 2007) to compare the ensemble of simulated DEMs and ice volumes with the reference.

     While the bias quantifies the mismatch between the expected value and the true value, CRPS compares a single true value x

210 with a cumulative distribution function (CDF) F:

$$\text{CRPS}(F,x) = \int_{-\infty}^{+\infty} \left(F(y) - \mathbf{1}(y > x) \right)^2 dx,$$

where $\mathbf{1}(y > x) = 1$ if $y > x$, and 0 otherwise. CRPS is equal to zero when the prediction is deterministic and equal to the true value. When the prediction displays a sharp distribution well centered around the reference, the CRPS is small. If the prediction displays a broader distribution or if the reference is out of the range of predicted values, the CRPS will be larger.

215   In the following subsections, we define the scores that were applied to the synthetic test cases. Note that to form final scores, each presented score is averaged over all the 20 synthetic test cases.

2.5.1 Ice volume comparison

For all the test cases, we define the ice volume by fixing (arbitrarily) the altitude z_c of the ice cap to the maximum altitude of the corresponding zone plus 4 m. The reference DEM is refereed as z_{ij}^{true}, with $i = 1, \ldots, I$ and $j = 1, \ldots, J$ coordinates (spatial

220 indexes). The ensemble of the simulated topographies are denoted z_{ij}^{s} where $s = 1, \ldots, S$ is the simulation index, and S the number of simulations.

     The volume of ice V_s for a given simulation is computed as the sum of the differences in altitude between the ice-cap altitude and the simulated topography times the area A covered by a grid cell (resolution):

$$V_s = \sum_{i,j} \left(z_{ij}^{s} - z_c \right) \times A. \tag{4}$$

225   The mean value of V_s over the ensemble of N_s simulations is an estimate of the expected value for the volume. We then compute the bias of the estimated value as the difference between the mean value with the reference volume and we take its absolute value. To simplify the computations and facilitate comparisons, the absolute value of the bias for the ice volume is considered per unit area. The elevation of the glacier surface is known, therefore the absolute bias on the volume estimate

depends only on the basal elevation simulations:

$$\text{AB(volume)} = \frac{1}{IJ} \left| \sum_{i,j} \left[\left(\sum_s \frac{z_{ij}^s}{N_s} \right) - z_{ij}^{\text{true}} \right] \right|. \tag{5}$$

Following the same logic, the CRPS score of the volume prediction is computed by first summing the elevation values in the domain $y_s = \sum_{ij} z_{ij}^s$ for each simulation. The CDF of these y_s values is denoted Y, and $y^{\text{true}} = \sum_{ij} z_{ij}^{\text{true}}$. Then the CRPS of the volume estimation is given by:

$$\text{CRPS(volume)} = \frac{1}{IJ} \text{CRPS}(Y, y^{\text{true}}). \tag{6}$$

2.5.2 DEM comparison

To test if the altitude is properly estimated in all locations of the domain, we compute the absolute value of the bias at each location: it is defined as the absolute difference between the mean DEM (ensemble average over all the simulations) and the reference. To form a single score, this map is averaged over all points in the domain. The mean absolute bias (MAB) for the DEM estimations are therefore defined as follows:

$$\text{MAB(DEM)} = \frac{1}{IJ} \sum_{i,j} \left| \left(\sum_s \frac{z_{ij}^s}{N_s} \right) - z_{ij}^{\text{true}} \right|. \tag{7}$$

The units of MAB(DEM) and AB(volume) are identical. This allows to compare directly ice volume errors with DEM errors. Furthermore, MAB(DEM) provides an upper bound for AB(volume).

To compute the CRPS score, let us consider that at each point with indexes (i,j) a geostatistical method predicts a distribution of elevation values. The set $\{z_{ij}^1, z_{ij}^2, \ldots z_{ij}^S\}$ contains samples drawn from this distribution. Let Z_{ij} be its cumulative distribution function (CDF). It can be approximated by these samples. The mean CRPS of DEM (averaged over all locations) is given by:

$$\text{CRPS(DEM)} = \frac{1}{IJ} \sum_{i,j} \text{CRPS}(Z_{ij}, z_{ij}^{\text{true}}). \tag{8}$$

2.5.3 Flow accumulation comparison

Flow accumulation is considered here because often DEM are used to make predictions that are highly affected by its geomorphological structures or its roughness. Predicting properly the geomorphological patterns of a DEM is critical for example to estimate the velocity at which the glacier may move or to simulate how melt water can be channelized at the base of the glacier. Flow accumulation maps are thus used in this study because they can be computed rapidly and easily and more importantly they illustrate well the concept of complex geomorphological/roughness description. A flow accumulation map represents in each cell the number of cells that are located upstream (e.g. Tarboton et al., 1991). They are computed by first estimating the flow directions from the local gradients of altitude and integrating the number of cells along the flow path. A very bumpy

topography, with many local minima, will lead to small values of accumulation. A smooth topography will lead to more contin-uous paths and higher accumulation values. The accumulation is calculated using the Pysheds open source code[1] for watershed delineation.

To quantify these differences, the probability density function (PDF) of the flow accumulations for each individual simulation
260 is compared with the PDF of the reference. A standard indicator to compare two PDFs P and Q is the Jensen-Shannon divergence (JSD). It is defined as follows:

$$\text{JSD}(P||Q) = \text{KLD}(P||M)/2 + \text{KLD}(Q||M)/2, \tag{9}$$

with $M = (P + Q)/2$ and KLD representing the Kullback-Leibler divergence (e.g. MacKay, 2007).

Supposing that the flow accumulation map is given by f_{ij}^{true} for the reference and by f_{ij}^s for the simulation s. The probability
265 distributions are created from the flow maps in the following way. First, the set of $K = 14$ bins are defined: $\{B_1, \ldots, B_K\}$:
$B_1 = (0, 1]$ and $B_k = (2^{k-2}, 2^{k-1}]$ for $k \in \{2, \ldots, K\}$. Each bin is an interval. We then define F_k, the counts of elements f_{ij} which fall into the interval B_k, that is:

$$F_k = \sum_{ij} \mathbf{1}(F_{ij} \in B_k) \tag{10}$$

with $\mathbf{1}(F_{ij} \in B_k) = 1$ if $F_{ij} \in B_k$, and 0 otherwise. The counts F_k are normalized so that $\tilde{F}_k$ satisfies: $\sum_k \tilde{F}_k |B_k| = 1$, where
270 $|B_k|$ is the length of interval B_k. The function $F : \mathbf{R} \to \mathbf{R}$ defined by: $F(x) = \tilde{F}_k$ if $x \in B_k$, and 0 otherwise, is a probability distribution function.

Let us call F^{true} such a PDF constructed from the reference flow accumulation map and $\{F^s, \quad s = 1, \ldots, S\}$ the family of PDFs constructed from the simulated DEMs. Then, the mean JSD of flow accumulation is given by:

$$\text{MJSD} = \sum_s \text{JSD}(F^s, F^{\text{true}}). \tag{11}$$

275 ## 2.6 Tsanfleuron and Scex Rouge basal topography estimation

The last step consists in applying the MPS and SGS simulations methods as well as kriging to the actual data set below the Tsanfleuron and Scex Rouge glaciers. The conditioning data are identical for the three methods: the GPR data below the glacier and the DEM around the glacier to ensure the continuity between the border of the simulated area and the exposed altitude of the glacier.

280 For the MPS simulations, we use the parameters and setup described in detail in section 2.2. We activate the multi-resolution option (Gaussian pyramids), the relative patterns search, and use the topography gradient as a secondary variable. This time, only three sets of parameters are used: the ones producing the best scores during the systematic comparison. The training data set is the complete exposed part of the glacier's bedrock as a primary variable and its computed gradient as secondary variable. The DEM is also used directly as hard conditioning data. In total, 120 MPS simulations (40 simulations per parameters set) are
285 generated.

---

[1]https://github.com/mdbartos/pysheds

The Cryosphere
Discussions

For the sequential Gaussian simulations and the kriging estimate, the variogram that is employed is the one introduced earlier in section 2.3. Both methods use a search ellipsoid of 1500 m and 24 neighbors for the conditioning. 40 SGS simulations are generated.

The ice volumes are then computed between all the simulated basal surfaces and the ice topography measured in august
290   (end of summer) 2011 and 2019. For 2011, we use the Alti3D DEM from the Swiss federal office of topography, and our DEM for 2019. For 2019, we use the DEM that was acquired in this work (see section 2.1). The statistics of the volumes are then computed for each methods. The standard deviation of the simulated values is used to provide the uncertainty range (2σ) of the volume. This uncertainty range takes into account only the uncertainty resulting from the spatial variability of the bedrock and its interpolation using an incomplete data set. These estimations do not encompass the other possible sources of
295   error/uncertainty that can arise from the GPR data acquisition (picking, time to depth conversion) or for the DEM acquisition. Finally, the flow accumulations are computed for all the simulations.

3   Results of the systematic comparison

Figure 5 shows a 3D perspective view of the topographies obtained from one of the 20 test cases. Figure 5a shows the reference DEM for that case, fig.5b-d show one example of MPS simulation, SGS simulation, and the kriging estimation respectively. As
300   expected, the kriging estimation produces the smoothest and the SGS the roughest topography. The MPS simulation, fig.5b, is characterized by an intermediate roughness. As compared to the reference, and as expected, kriging underestimates the small local variations. On the opposite, the SGS topography is rougher than the reference, the complex features of the geomorphology are not properly reproduced even if the large patterns/trends are correctly simulated. The MPS simulation shows more realistic patterns that are continuous and the simulated features appear visually close to the true DEM patterns.
305   Figure 6 shows the results for 4 test cases among the 20 that we conducted. The figure is organized as a table. Each line corresponds to one test case. The first column (Fig. 6a) shows the unknown topography for each case, and the black horizontal line indicates the position of the cross section used to display some results in Figs. 6b and 6c The last column (Fig.6d) represents the histograms of volume estimations as compared to the reference for each case.

Regarding the cross-sections, Fig. 6b shows the results for the MPS technique and Fig. 6c shows the results for the Kriging
310   and SGS methods. The red curve is the reference in all cases. The predictions are represented by the mean and the 2σ interval estimated from the ensemble of MPS and SGS simulations. The first observation is that the true altitude generally lies very well within the uncertainty range predicted by the different methods. The uncertainty is small on the sides of the domain because the altitude is known at those locations. We observe, that the uncertainty is generally larger with the SGS method than with MPS. This observation can be explained by the fact that even if both methods use the same number of conditioning data, the
315   MPS method is more constrained by the training image and the associated secondary gradient variable. We also observe that the reference topography is sometimes outside of the 2σ interval, while the SGS distribution always contains the reference. Since the 2σ interval corresponds roughly to a 95% confidence interval, it is expected that in 5% of the simulated cases, the reference altitude should fall outside of the prediction range. Therefore, we argue that the uncertainty estimated with the SGS
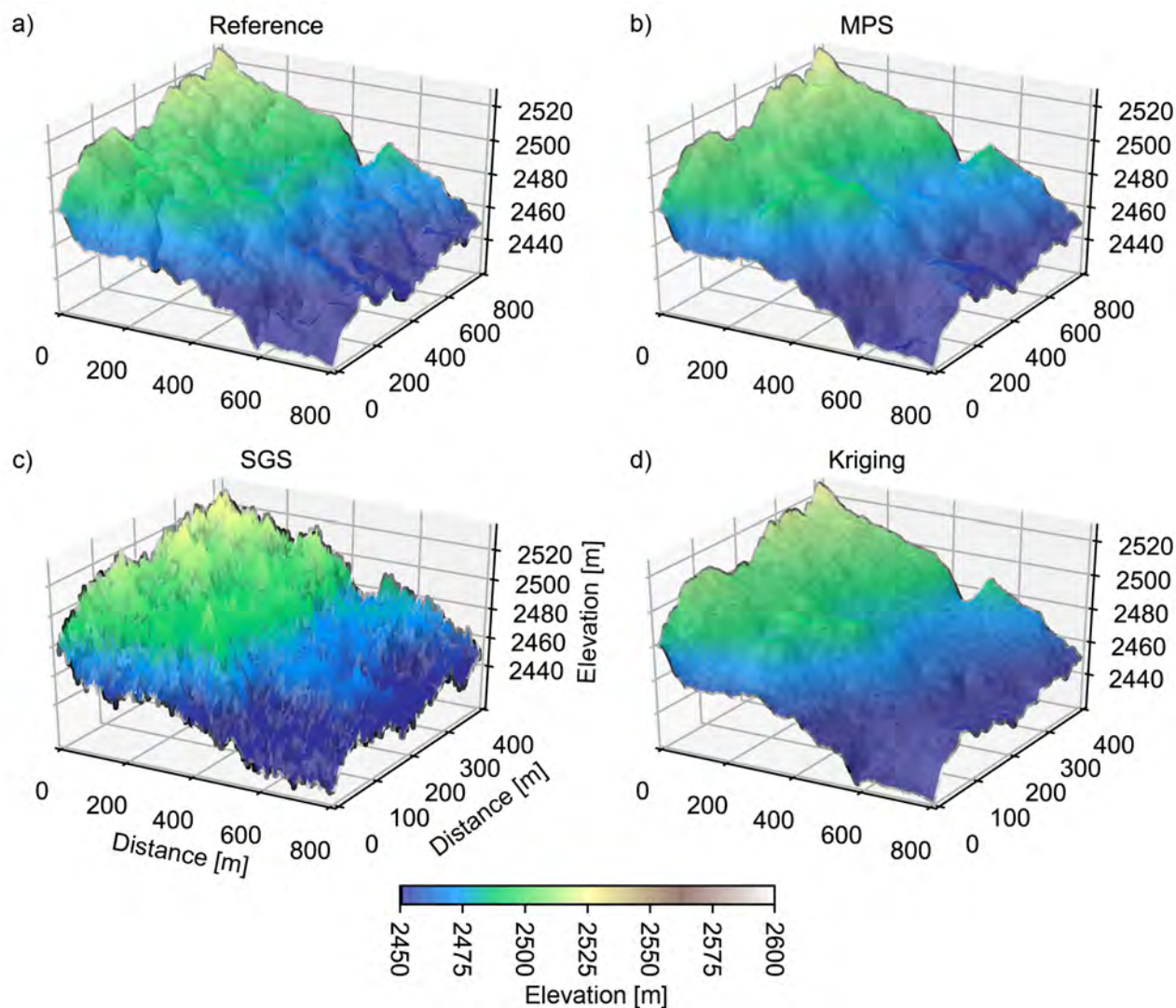
Figure 5. 3D view of topographic interpolation from the synthetic test case. The color correspond to the simulated elevation. a) presents the reference topography of the test case. b) a MPS simulation, c) a SGS simulation and d) a corresponding kriging estimate. The roughness is overestimated in with the SGS and underestimated with the kriging estimation. MPS simulation provide an acceptable compromise between the method and produce realistic structures.

simulations is too large while the one obtained with MPS is more reasonable. Finally, as expected, the kriging produces a
320   smooth curve that does not represent the small-scale variations in topography but reproduces very well and efficiently the mean
of the ensemble (the expected value of the altitude in a statistical sense) and therefore reproduces well the general trend of the
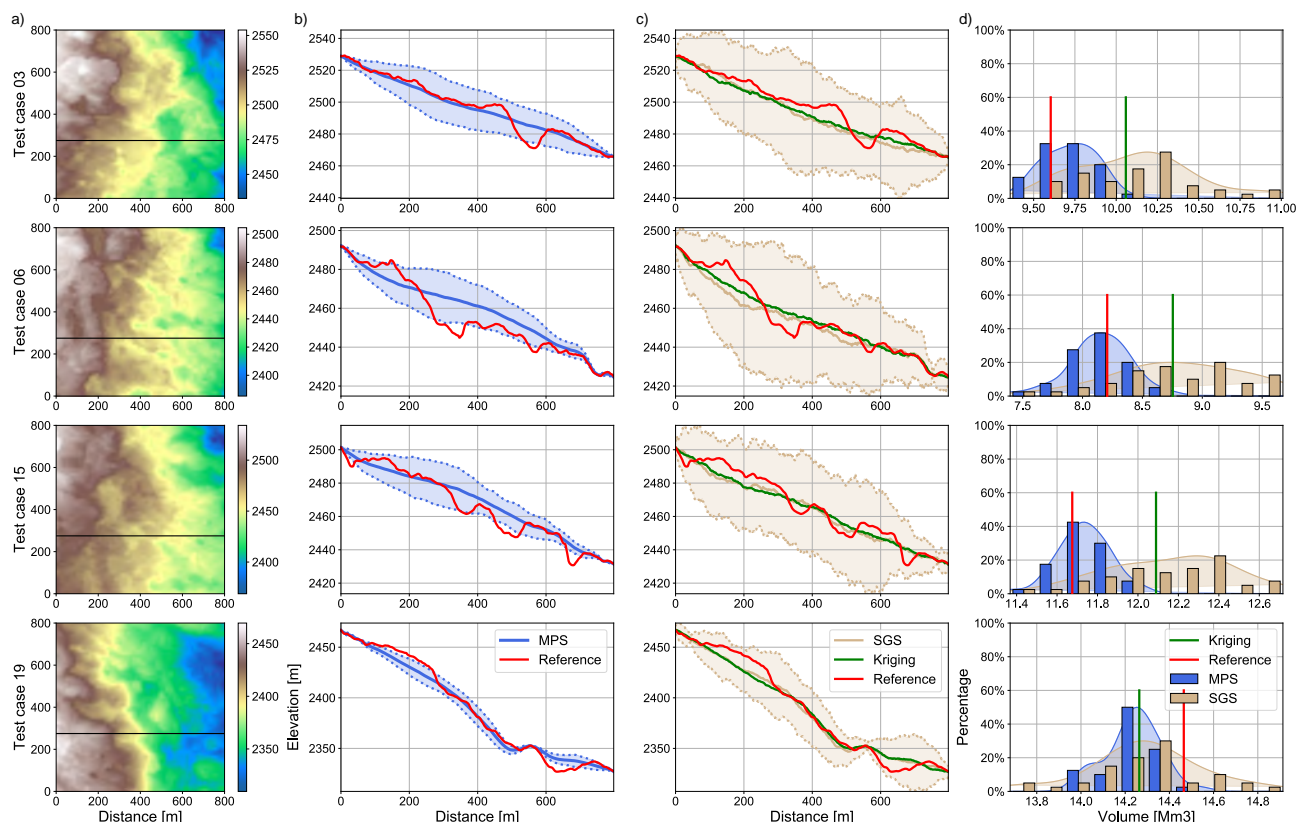basal elevation.

14

Figure 6. Synthetic test results. a) displays the reference DEM on a plan view, the black line showing the location of the cross sections. b) presents the distribution of the cross section simulated with the MPS method (parameter set 3). c) presents the distribution of the cross section simulated with the SGS methods (parameter set 1). d) presents the different volume distribution of the methods against the reference one in red.

Regarding the volume, Fig. 6d shows first that both the SGS and MPS volume estimations contain the reference within their uncertainty range. The red line always lies inside the histograms predicted by the two methods. The volumes estimated by kriging are, again as expected, close to the mean of the volumes obtained from the SGS simulations. However, the volumes estimated by kriging can over or under estimate the reference, and the method does not provide an error estimation. When looking more precisely at Fig. 6d, we observe a higher variability for the SGS method. The MPS volume distributions are better centered around the true volumes. For the SGS volume distributions, the mean is generally less close to the reference than with the MPS method. These observations are confirmed by the CRPS scores of the SGS simulations that are lower than the ones of the MPS simulations (Tab. 2).

The quality scores presented in table 2, show that all of the MPS simulations with different parameter sets performed better than the SGS sets for almost all of the indicators calculated. The scores are the closest between the methods regarding the average volume estimated, signifying that on average all the methods perform well to estimate a global volume. However,

15

Table 2. Quality indicators averaged over all realizations for different simulation methods (MPS, SGS, kriging) and for different parameter sets. The rows are sorted by best (lowest) CRPS score of ice volume estimation. CRPS score of ice volume estimation, mean absolute error of the ice volume, CRPS score of DEM averaged over all points, mean absolute error of DEM averaged over all points, and Jensen-Shannon divergence of flow accumulation distributions averaged over all simulations.

Method	Set	CRPS(volume)	AB(volume)	CRPS(DEM)	MAB(DEM)	MJSD
MPS	6	1.41	2.01	3.59	4.96	0.014
	3	1.42	1.91	3.66	4.92	0.013
	8	1.47	2.04	3.64	5.01	0.015
	7	1.53	2.11	3.68	5.07	0.015
	5	1.60	2.14	3.79	5.06	0.014
	4	1.61	2.11	3.79	5.06	0.014
	0	1.62	2.06	3.88	4.98	0.018
	2	1.70	2.11	3.95	5.05	0.019
	1	1.70	2.11	3.95	5.05	0.019
SGS	0	1.97	2.86	4.17	5.54	0.109
	1	1.99	2.96	4.18	5.61	0.111
Kriging	0	2.91	2.91	5.45	5.45	0.047

larger differences between the methods can be observed when looking at the CRPS scores or the pointwise scores. The fact
335 that the MPS performed better in the CRPS score is due to the distributions of volumes that are more precise for MPS than for SGS.

Another important indicator to take into account is the mean Jensen-Shannon divergences of the flow accumulation scores. The scores of the MPS sets are ten times better than the score of the SGS and four times better than kriging. Figure 7 shows the different flow accumulation probability density distributions for one test case and for the different methods. SGS performs
340 poorly to reproduce the true probability density distribution, it misses the large flow accumulation values. Kriging, provides surprisingly a better distribution in these examples. Because kriging is smoother it tends to over create larger flow accumulation values. The MPS probability density curve is the closest to the true DEM one and implies a good performance in pattern reproduction.

Finally, the systematic tests showed that the best parameter sets were the number 6, 3 and 8 for MPS, and the 24 neighbors
345 parameter set for SGS. These parameters were then used for the practical application of the Tsanfleuron glacier.

4 Tsanfleuron glacier results

Figure 8 shows the comparison between the basal topography interpolated using SGS, kriging and MPS on a map view and along two cross-sections through the glacier. The mean global shape produced by the 3 methods are similar. The SGS sim-
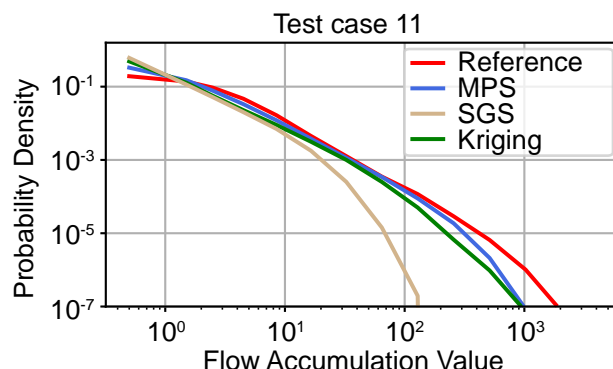
Figure 7. Probability distributions of flow accumulation values for example realisation #11. The probability distribution of flow accumulation for the true DEM is compared to an example MPS simulation, kriging map and SGS simulation. The corresponding Jensen-Shannon divergences with respect to the true distribution are: 0.015 (MPS), 0.228 (kriging), and 0.107 (SGS).

Table 3. Volumes of ice computed with the 2019 and 2011 DEM for the Tsanfleuron and Scex Rouge glaciers.

Method	Tsanfleuron 2019 [$mio\ m^3$]	2011 [$mio\ m^3$]	Scex-Rouge 2019 [$mio\ m^3$]	2011 [$mio\ m^3$]	Total 2019 [$mio\ m^3$]	2011 [$mio\ m^3$]
MPS	109.8 ± 1.5	143.2 ± 1.5	4.1 ± 0.3	6.6 ± 0.4	113.9 ± 1.6	149.8 ± 1.6
SGS	109.7 ± 1.7	143.3 ± 1.8	4.2 ± 0.2	7.05 ± 0.2	113.9 ± 1.8	150.4 ± 1.8
Kriging	109.0	143.0	4.1	6.8	113.1	149.9

ulations tends to be a little bit noisier, but in terms of expected value (mean value), the figure does not show any significant
350   difference between the methods.

Table 3 provides the estimated ice volume and uncertainties. The results from the three methods are very close: between 113 and 114 million cubic meters for 2019. With Kriging, it is not possible to estimate the uncertainty range on the volume. But with the SGS and MPS simulations, we obtain similar uncertainty ranges in the order of 1% for the volume. For comparison, and to evaluate the ice loss between 2011 and 2019, we also compute the volumes in 2011. The 2011 and 2019 surface DEM
355   were both acquired in August. According to the simulations, the Tsanfleuron and Scex Rouge glacier lost about 25% of their total ice volume in 9 years.

So far, the results obtained by the three methods are very close, because the differences in the spatial distribution of the basal elevation values are compensated when we integrating them over the whole glacier area to compute the volume or mean altitude.

360   However, the flow accumulation results (Fig. 9) are very different and highly affected by the detailed geomorphological structures in the interpolated surfaces. The SGS simulations lack realism in this case and cannot predict the high flow accumulations. They are limited to short paths, with many local minima due to an overestimation of the roughness of the simulated topographies. On the other hand, kriging provides an interpolated topography that is smoother than the reality and overesti-
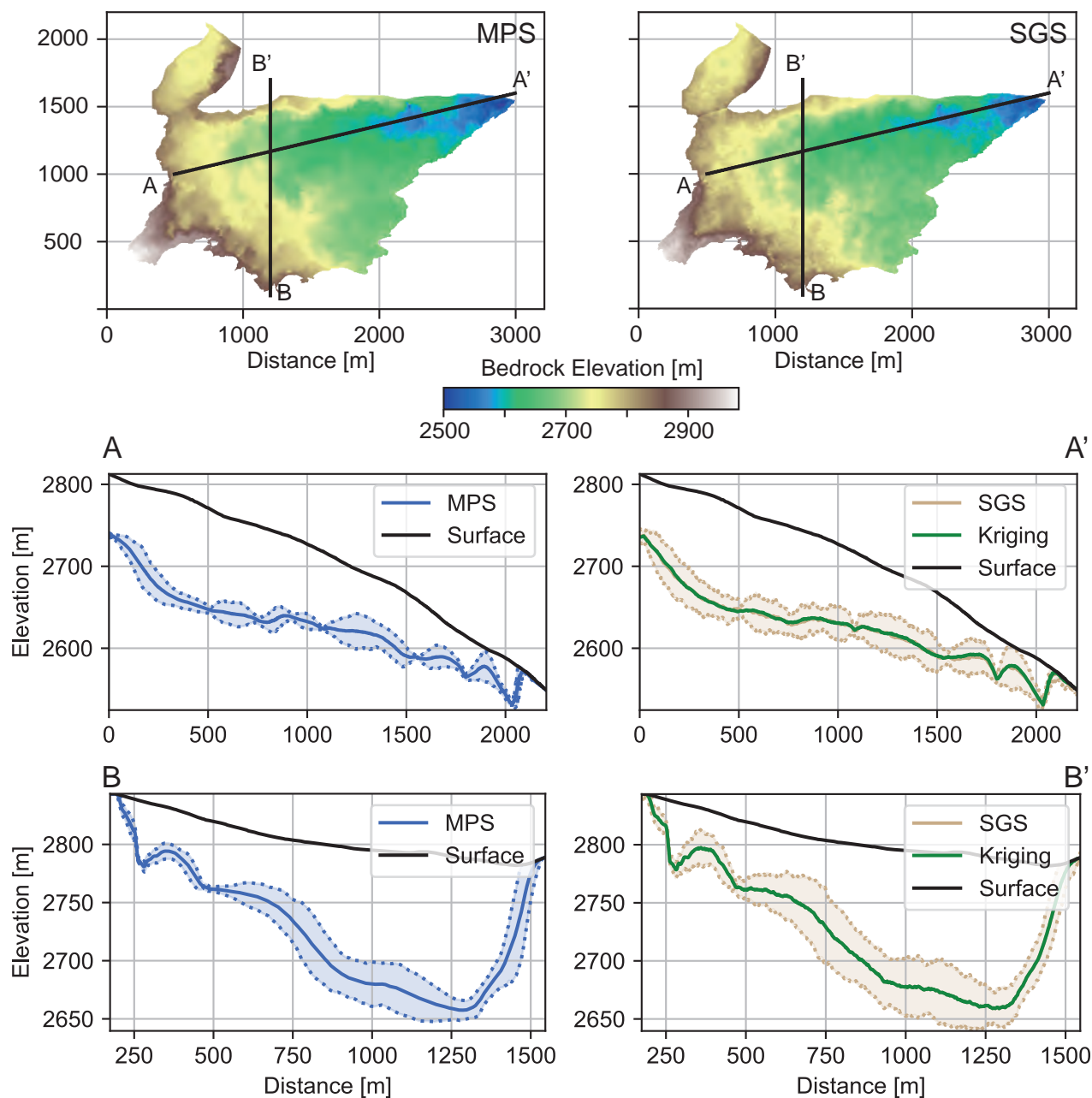
Figure 8. Simulated basal topography for the MPS method (in blue) and for the SGS method (in brown). The kriging estimated topography is displayed along side the SGS simulation in green .

mates the flow accumulations. Finally, MPS is able to generate more realistic basal topographies. The predicted topographies
365 display geomorphological features and roughness that are similar to the structures visible in the uncovered bedrock area.
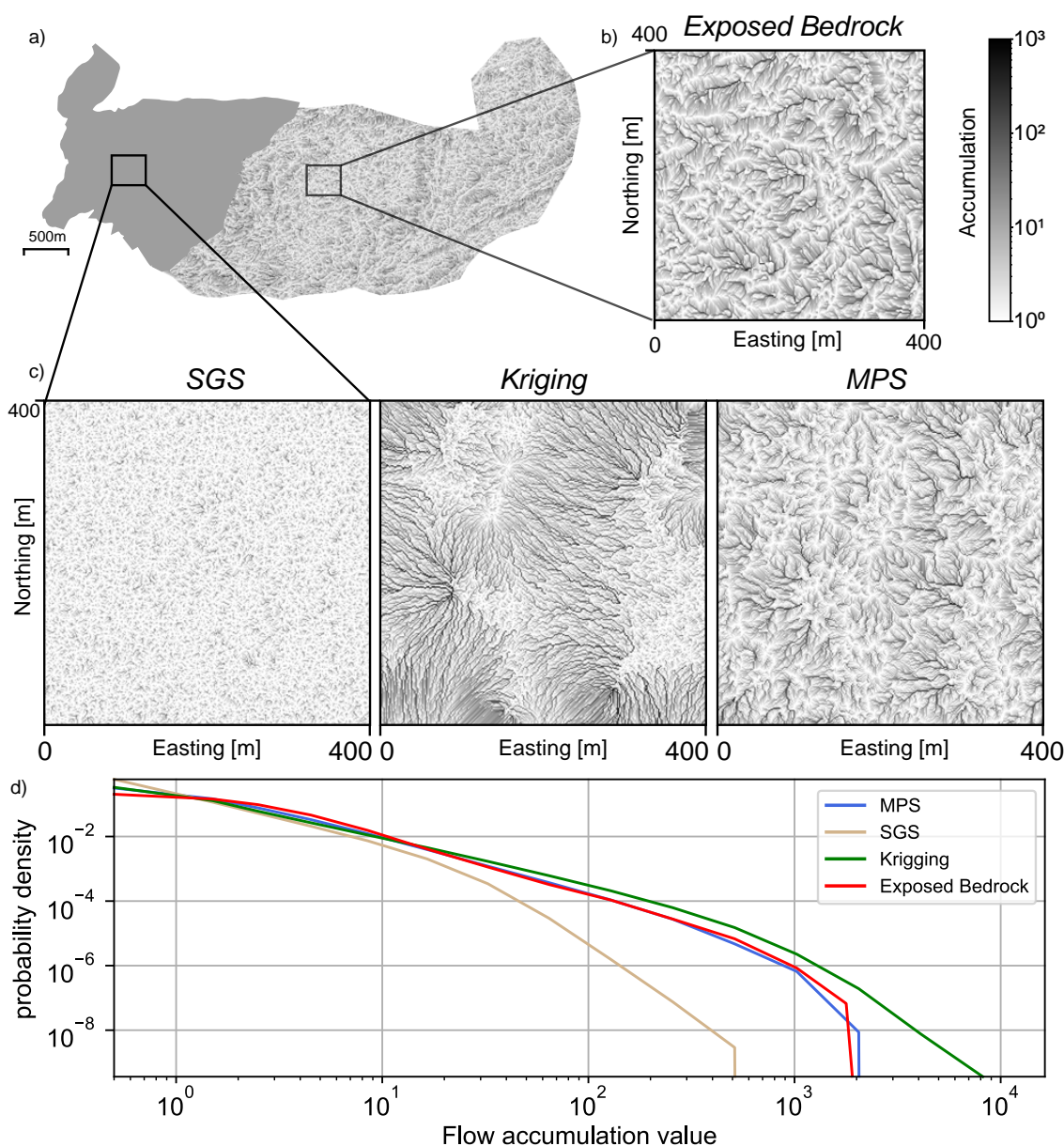
Figure 9. Flow accumulations calculated from the 3 methods and compared against the one computed in the exposed part of the bedrock used as reference, and the probability density of accumulation values. The SGS simulation under-estimates the length of the connected path, while kriging over-estimates it. The visual patterns and the flow accumulation distribution obtained with MPS are the closest to the exposed bedrock reference.

5 Discussion

5.1 MPS parametrization

When comparing the interpolated basal topographies with the three methods, our results show that the MPS approach provides the simulations that display geomorphological features that are the closest with the data set. But to obtain those results, the

370 DeeSse algorithm needs to be properly parametrized and adequate secondary variables have to be used. During this project, we have tested various options. Using the topography gradient as a secondary variable proved to be a simple and efficient solution. But further improvements could certainly be made. One possibility that we considered but did not implement would be to use as secondary variables two hillshades projection 45 degrees apart from each other. Adding these two variables would allow to account both for the absolute steepness of the topography but also to the orientation in space of the geomorphological patterns.

375 5.2 Ice volume of the Tsanfleuron glacier

The results from the previous section shows that the three geostatistical methods are able to provide consistent and comparable estimates of the mean basal topography and the overall ice volume. This similarity is expected for the SGS and kriging because the volume calculation is a linear function of the basal topography, and in this situation kriging and simulations will provide the same mean value (see e.g. Chiles and Delfiner, 2012). It was not obvious that MPS would also provide the same volume

380 because the underlying spatial variability model is different. Kriging and SGS are based on the same variogram model, but MPS is based on the complete topographic data set and is accounting for higher order statistics. The fact that the three techniques provide a consistent result is therefore an interesting finding. At the glacier scale, the spatial distributions of the thicknesses (fig. 10) according to the three methods is consistent. The thickest area is in the northern part of the Tsanfleuron area, and present a roughly E-W orientation.

385 Only the SGS and MPS methods are able to estimate the uncertainties on the total volume. The volume uncertainties estimated with a multiGaussian model are in general reliable (see e.g. Chiles and Delfiner, 2012). Here, we show that the uncertainties obtained with the MPS are consistent with those obtained with SGS.

For the Scex Rouge and Tsanfleuron glacier these three methods allow to obtain an estimation 149.8 ± 1.6 million cubic meters of ice for 2011. This result is larger than the 100 million cubic meters estimated by Gremaud and Goldscheider (2010)

390 for 2008. We explain this difference by considering that Gremaud and Goldscheider (2010) employed a different geophysical technique and had less data points over the glacier to interpolate the ice thickness (using kriging). More precisely, they used a radio magneto telluric geophysical method; they also inverted the geophysical signal using two layers assumptions, one representing the glacier and the other the underlying limestone. The authors indicate that they may have underestimated the actual thickness of the glacier. It could be due to an erroneous estimation of the electrical resistivity of the glacier possibly

395 affected by the presence of meltwater. Another geophysical campaign was conducted by Nath Sovik and Huss (2010). They report much deeper ice thickness reaching up to 180 meters in the central part of the glacier. Personal communication with these authors indicate that they are uncertain about the very deep data, they obtain a volume in the order of 200 million cubic meters for the Tsanfleuron glacier only in 2009.
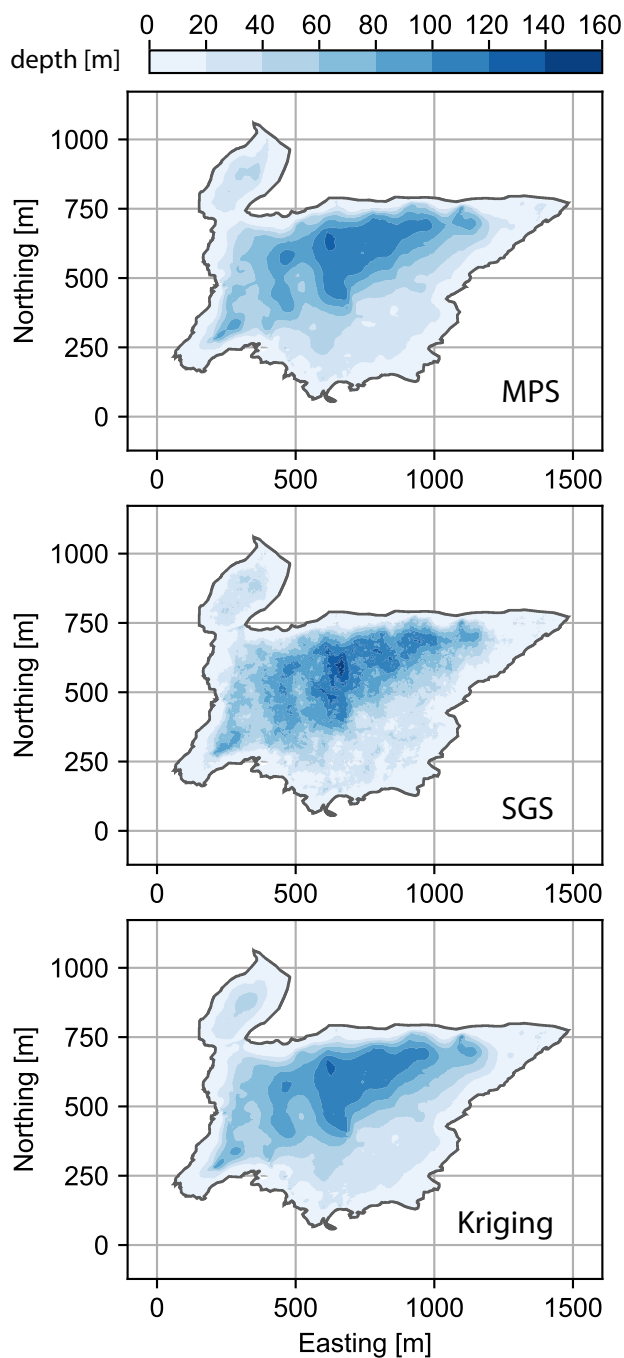
The Cryosphere
Discussions

Open Access

EGU

Figure 10. Ice thickness calculated from the 3 methods using the 2019 surface DEM. The SGS and the MPS basal models used are the averaged model over all the realisations.

Another indirect comparison with existing data was made using year-to-year mass balance (GLAMOS-Glacier Monitoring

400 Switzerland, 2019). An ice density value of 850 ± 60 kg/m^3 was used as recommended in Huss (2013) to perform the conversion between water equivalent (w.e.) and ice volume. With this method, the loss of volume is estimated to be around 34 ± 2.5 $Mio\ m^3$ of ice between September 2011 and 2019. This value is similar to the one we derived with our approach (35.9 ± 3.2 $Mio\ m^3$ for the MPS). We note that a linear extrapolation of this loss, obviously inaccurate due to all the effects that are not considered in this extrapolation, indicates that the glacier will disappear in about 30 to 40 years.

405 To finalize that part of the discussion, we would like to recall that several operators did the picking of the depth of the reflectors independently on our GPR data and that we randomized the order in which the data were presented to the operator. We also compared the result of the picking from the different operators and removed the part of the data that were not consistent. Even if the surface and volume estimations may still suffer from some remaining errors, we tried to apply these strict procedures to avoid bias and therefore, we expect that the data set and the estimated volumes should be as reliable as possible. As we wrote

410 earlier, some additional sources of errors were not considered in the computation of the uncertainty on the glacier volume. One of these error sources is the topography of the surface of the glacier, another one is the velocity used to convert the two way time data from the GPR into depth. We did not include them in our comparison because we wanted to compare only the effect of the interpolation methods. All these additional sources of error are identical for the different methods.

5.3 Which geostatistical method for which purposes?

415 To estimate rapidly the volume of ice, our results show that the kriging method provides a value that this reasonnable. However, kriging cannot be used to obtain directly the uncertainty on the volume.

We argue that any scientific estimation should always be accompanied by an uncertainty estimation, it is therefore preferable to use directly the SGS or MPS approach to get not only the volume but also the corresponding uncertainty. The two methods provide comparable results. The SGS methods requires to infer a variogram model from the experimental variogram of the

420 data. On the opposite, the MPS method requires simply to provide an exhaustive data set that represents the type of spatial variability that is analog to the patterns that are expected below the glacier. In a previous study (Dagasan et al., 2019), we have shown for a different application that even if the training data are slightly different from the spatial patterns that are actually occurring at the site of interest, it is possible by cross-validation to adjust the parameters of the MPS simulation to compensate for this mismatch and obtain satisfying results.

425 Finally, if the estimated topographies of the bedrock below the glacier have to be used to estimate a quantity that derives non linearly from the topography, the MPS method should be used. Inded, we have shown that MPS provides a much better reproduction of the geomorphology of the simulated basal surfaces: the results are much closer from the reference than the other two techniques. This result confirms the observations made by MacKie et al. (2020) concerning the importance of using MPS for the estimation of the presence of underglacial lakes. The importance of simulating properly the roughness of

430 subglacial topography was also already highlithed by Goff et al. (2014) who used a combination of multigaussian simulations with deterministic trends, but the procedure that we propose with MPS is somehow simpler to implement.

6   Conclusions

Ice volume estimation is complicated, but yet capital. Combined with mass balance estimation, they can provide a priceless estimation of the number of years remaining for a glacier before its melting.

435   This study proposes an example of the benefits of using advanced geostatistical methods for basal topography simulation. MPS approach managed to produce highly realistic basal structures, even in areas where the data are scarce or the structure complex. In addition, such method can also indicate where to perform further measurements in order to reduce the uncertainty on the volume estimation. On the other hand, mean SGS and kriging tend to produce a smoothed model, that can lack precision when trying to use the interpolated basal topography for flow equations or risk assessments. In these cases, the secondary

440   structures may be even more important than the primary global trend.

However, It is important to note that MPS approach can be sometimes tricky to use due to the selection or creation process of the TI. The method is only that efficient when proper TI, similar to the glacier basal structures is available. Finding some analogs data is an important part of the approach and has a major impact on the simulation outputs. It may be difficult to apply this method in steeper valleys, where sediment tends to cover the bedrock making TI selection complex.

445   The ice volumes calculated for the Scex Rouge and Tsanfleuron glacier are in accordance with the mass balance calculation and are linked with robust error estimation.

Finally, when applying existing mass balances to our volume estimation, we were able to draft a possible evolution of the glacier in the context of global warming. The results and the approximation of the glacier end of life could be important for global awareness, political decisions, and preparing the mountains' infrastructures for its next evolution.

450   A further work that could be carried on these data is the estimation of variation of surface in the future. Using the bedrock model and a melting model, it is possible to predict the variation, in terms of the area, of the glacier and therefore better predict the future melting.

In addition, the bedrock model could be used to detect possible karstic inflow in the basement of the glacier. This would be capital in order to predict the effect in the following years of the glacial retreat and on the availability of groundwater in the

455   valley.

Author contributions.   A.N. coordinated and conducted a part of the field work. A.N. processed the GPR and drone data. A.N., V.D., J.S. and P.R. designed and tested the different geostatistical procedures. A.N. and V.D. prepared the data. P.J. participated in the data acquisition,

460   designed and implemented the quality indicators. A.N., V.D. and P.J. wrote the paper. P.R. initiated and supervised the work, conducted the field acquisition, and was involved in the writing, and editing of the paper.

References

Berthier, E., Vincent, C., Magnússon, E., Gunnlaugsson, A. T., Pitte, P., Le Meur, E., Masiokas, M., Ruiz, L., Pálsson, F., Belart, J. M. C., and
   Wagnon, P.: Glacier topography and elevation changes derived from Pléiades sub-meter stereo images, The Cryosphere, 8, 2275–2291,
   https://doi.org/10.5194/tc-8-2275-2014, 2014.

470 Bohleber, P., Sold, L., Hardy, D. R., Schwikowski, M., Klenk, P., Fischer, A., Sirguey, P., Cullen, N. J., Potocki, M., Hoffmann, H., and
   Mayewski, P.: Ground-penetrating radar reveals ice thickness and undisturbed englacial layers at Kilimanjaro's Northern Ice Field, The
   Cryosphere, 11, 469–482, https://doi.org/10.5194/tc-11-469-2017, 2017.

Chiles, J.-P. and Delfiner, P.: Geostatistics: Modeling Spatial Uncertainty, Second Edition, vol. 497 of *Wiley Series in Probability and Statis-
   tics*, John Wiley & Sons, Hoboken, New Jersey, USA, 2012.

475 Chudley, T. R., Christoffersen, P., Doyle, S. H., Abellan, A., and Snooke, N.: High-accuracy UAV photogrammetry of ice sheet dynamics
   with no ground control, The Cryosphere, 13, 955–968, https://doi.org/10.5194/tc-13-955-2019, 2019.

Dagasan, Y., Erten, O., Renard, P., Straubhaar, J., and Topal, E.: Multiple-point statistical simulation of the ore boundaries for a lateritic
   bauxite deposit, Stochastic Environmental Research and Risk Assessment, 33, 865–878, 2019.

Dall'Alba, V., Renard, P., Straubhaar, J., Issautier, B., Duvail, C., and Caballero, Y.: 3D multiple-point statistics simulations of the Roussillon
480   Continental Pliocene aquifer using DeeSse, Hydrology and Earth System Sciences, 24, 4997–5013, 2020.

de Carvalho, P. R. M., da Costa, J. F. C. L., Rasera, L. G., and Varella, L. E. S.: Geostatistical facies simulation with geometric patterns of a
   petroleum reservoir, Stochastic Environmental Research and Risk Assessment, 31, 1805–1822, https://doi.org/10.1007/s00477-016-1243-
   5, 2016.

Eisen, O., Nixdorf, U., Wilhelms, F., and Miller, H.: Electromagnetic wave speed in polar ice: validation of the common-
485   midpoint technique with high-resolution dielectric-profiling and γ-density measurements, Annals of Glaciology, 34, 150–156,
   https://doi.org/10.3189/172756402781817509, 2002.

Flowers, G. E. and Clarke, G. K. C.: Surface and bed topography of Trapridge Glacier, Yukon Territory, Canada: digital elevation models
   and derived hydraulic geometry, Journal of Glaciology, 45, 165–174, https://doi.org/10.3189/s0022143000003142, 1999.

Frey, H., Machguth, H., Huss, M., Huggel, C., Bajracharya, S., Bolch, T., Kulkarni, A., Linsbauer, A., Salzmann, N., and Stoffel,
490   M.: Estimating the volume of glaciers in the Himalayan-Karakoram region using different methods, The Cryosphere, 8, 2313–2333,
   https://doi.org/10.5194/tc-8-2313-2014, 2014.

Gantayat, P., Kulkarni, A. V., and Srinivasan, J.: Estimation of ice thickness using surface velocities and slope: case study at Gangotri Glacier,
   India, Journal of Glaciology, 60, 277–282, https://doi.org/10.3189/2014jog13j078, 2014.

Gerlitz, K., Knoll, M. D., Cross, G. M., Luzitano, R. D., and Knight, R.: Processing Ground Penetrating Radar Data to Improve Resolution of
495   Near-Surface Targets, in: Symposium on the Application of Geophysics to Engineering and Environmental Problems 1993, Environment
   and Engineering Geophysical Society, https://doi.org/10.4133/1.2922036, 1993.

GLAMOS-Glacier Monitoring Switzerland: Swiss Glacier Mass Balance (release 2019), https://doi.org/10.18750/MASSBALANCE.2019.R2019,
   2019.

Gneiting, T., Balabdaoui, F., and Raftery, A. E.: Probabilistic forecasts, calibration and sharpness, Journal of the Royal Statistical Society:
500   Series B (Statistical Methodology), 69, 243–268, 2007.

Goff, J. A., Powell, E. M., Young, D. A., and Blankenship, D. D.: Conditional simulation of Thwaites Glacier (Antarctica) bed topography
   for flow models: Incorporating inhomogeneous statistics and channelized morphology, Journal of Glaciology, 60, 635–646, 2014.

Grab, M., Mattea, E., Bauder, A., Huss, M., Rabenstein, L., Hodel, E., Linsbauer, A., Langhammer, L., Schmid, L., Church, G., Hellmann, S., Délèze, K., Schaer, P., Lathion, P., Farinotti, D., and Maurer, H.: Ice thickness distribution of all Swiss glaciers based on extended

505   ground-penetrating radar data and glaciological modeling, Journal of Glaciology, pp. 1–19, https://doi.org/10.1017/jog.2021.55, 2021.

Gremaud, V.: Géologie du karst de Tsanfleuron, Collection EDYTEM. Cahiers de géographie, 7, 127–134, https://doi.org/10.3406/edyte.2008.1062, 2008.

Gremaud, V. and Goldscheider, N.: Geometry and drainage of a retreating glacier overlying and recharging a karst aquifer, Tsanfleuron-Sanetsch, Swiss Alps, Acta carsologica, 39, 2010.

510 Haugerud, R. A., Harding, D. J., Johnson, S. Y., Harless, J. L., Weaver, C. S., and Sherrod, B. L.: High-Resolution Lidar Topography of the Puget Lowland, Washington —A Bonanza for Earth Science, GSA Today, 13, 4, https://doi.org/10.1130/1052-5173(2003)13<0004:hltotp>2.0.co;2, 2003.

Huss, M.: Density assumptions for converting geodetic glacier volume change to mass change, The Cryosphere, 7, 877–887, https://doi.org/10.5194/tc-7-877-2013, 2013.

515 Journel, A. and Zhang, T.: The necessity of a multiple-point prior model, Mathematical geology, 38, 591–610, 2006.

MacKay, D. J. C.: Information theory, inference, and learning algorithms, Cambridge University Press, Cambridge, 6th printing edn., 2007.

MacKie, E. J. and Schroeder, D. M.: Geostatistically Simulating Subglacial Topography with Synthetic Training Data, in: IGARSS 2020 - 2020 IEEE International Geoscience and Remote Sensing Symposium, IEEE, https://doi.org/10.1109/igarss39084.2020.9324563, 2020.

MacKie, E. J., Schroeder, D. M., Caers, J., Siegfried, M. R., and Scheidt, C.: Antarctic Topographic Realizations and Geostatistical Modeling

520   Used to Map Subglacial Lakes, Journal of Geophysical Research: Earth Surface, 125, https://doi.org/10.1029/2019jf005420, 2020.

Mariethoz, G., Renard, P., and Straubhaar, J.: The Direct Sampling method to perform multiple-point geostatistical simulations, Water Resources Research, 46, https://doi.org/10.1029/2008wr007621, 2010.

Meerschman, E., Pirot, G., Mariethoz, G., Straubhaar, J., Van Meirvenne, M., and Renard, P.: A practical guide to performing multiple-point statistical simulations with the Direct Sampling algorithm, Computers & Geosciences, 52, 307–324, 2013.

525 Moorman, B. J. and Michel, F. A.: Glacial hydrological system characterization using ground-penetrating radar, Hydrological Processes, 14, 2645–2667, https://doi.org/10.1002/1099-1085(20001030)14:15<2645::aid-hyp84>3.0.co;2-2, 2000.

Nath Sovik, K. and Huss, M.: Glaciological investigations on three glaciers at Les Diablerets, Alpes Vaudoises, in: Abstract Volume. 8th Swiss Geoscience Meeting. Symposium 10. Open Cryosphere Session, pp. 243–244, Platform Geosciences, Swiss Academy Swiss Geoscience Meeting 2010 of Science, SCNAT, University of Fribourg, Switzerland, 2010.

530 Oriani, F., Straubhaar, J., Renard, P., and Mariethoz, G.: Simulation of rainfall time series from different climatic regions using the direct sampling technique, Hydrology and Earth System Sciences, 18, 3015–3031, 2014.

Plewes, L. A. and Hubbard, B.: A review of the use of radio-echo sounding in glaciology, Progress in Physical Geography: Earth and Environment, 25, 203–236, https://doi.org/10.1177/030913330102500203, 2001.

Schoeneich, P. and Reynard, E.: Structural Landscapes and Relative Landforms of the Diablerets Massif, in: Landscapes and Landforms

535   of Switzerland, edited by Reynard, E., World Geomorphological Landscapes, pp. 123–141, Springer, https://doi.org/10.1007/978-3-030-43203-4_9, 2021.

Straubhaar, J.: DeeSse user's guide, Tech. rep., The Centre for Hydrogeology and Geothermics (CHYN), University of Neuchâtel: Neuchâtel, Switzerland, 2019.

Straubhaar, J. and Renard, P.: Conditioning Multiple-Point Statistics Simulation to Inequality Data, Earth and Space Science, p.

540   e2020EA001515, https://doi.org/10.1029/2020EA001515, 2021.

Straubhaar, J., Renard, P., and Chugunova, T.: Multiple-point statistics using multi-resolution images, Stochastic Environmental Research and Risk Assessment, 34, 251–273, https://doi.org/10.1007/s00477-020-01770-8, 2020.

Tarboton, D. G., Bras, R. L., and Rodriguez-Iturbe, I.: On the extraction of channel networks from digital elevation data, Hydrological processes, 5, 81–100, 1991.

545   Vanlooy, J. A., Miège, C., Vandeberg, G. S., and Forster, R. R.: Ice volume estimation inferred from ice thickness and surface measurements for Continental Glacier, Wind River Range, Wyoming, USA, Journal of Glaciology, 60, 478–488, https://doi.org/10.3189/2014jog13j162, 2014.